Theor Chem Account (2008) 120:243–261
DOI 10.1007/s00214-007-0315-5

REGULAR ARTICLE

A theoretical study of the reaction of Ti^+ with propane

Jerzy Moc · Mark S. Gordon

Received: 3 January 2007 / Accepted: 16 February 2007 / Published online: 7 June 2007

Abstract Detailed quartet and doublet potential energy surfaces for the $Ti^+ + C_3H_8 \rightarrow TiC_3H_6^+ + H_2$ and $Ti^+ + C_3H_8 \rightarrow TiC_2H_4^+ + CH_4$ elimination reactions have been studied using density functional theory with B3LYP functional and ab initio coupled cluster CCSD(T) methods. Several H_2 elimination and CH_4 elimination reaction paths have been examined including the IRC following. In particular, the mechanisms involving, respectively, the $H_2TiC_3H_6^+$ and $CH_3TiHC_2H_4^+$ intermediates have been studied.

Keywords $Ti^+ + C_3H_8$ reaction · Density functional theory · CCSD(T)

1 Introduction

Gas-phase studies of bare transition-metal cations (M^+) with neutral substrates enable elucidation of the elementary reaction steps under well defined conditions, and they have been an active experimental research area [1–8]. This especially concerns activation of the prototypical C–H and C–C bonds by M^+. Because of the charged nature of intermediates and products of these activations, various mass spectrometric techniques have been the methods of choice to study such processes [1–8]. The lack of additional effects caused by solvents, other coordinated ligands, counterions, etc. make the gas-phase transition metal cation/molecule reactions also well suited for computational modeling, provided that the appropriate theoretical methods are used [9]. Previously, we investigated the reaction paths for the early transition metal cation Ti^+ and ethane using density functional theory (DFT) and single- and multi-reference ab initio methods [10]. The ethane C–H activation by Ti^+ resulting in the formation of $TiC_2H_4^+ + H_2$ was calculated to be essentially thermoneutral, while the C–C activation leading to the formation of $TiCH_2^+ + CH_4$ appeared to be a significantly endothermic process with all the computational methods used [10]. In the present work, we extend these theoretical studies to the Ti^+ + propane mechanism. From the mechanistic point of view, the bond activation of propane by a transition metal cation is a more complex process compared to that of ethane because, both primary and secondary C–H bonds can be attacked by M^+ in propane. Unlike the lower alkanes, the exothermic C–C bond activation channel might be available with the propane substrate [1–3].

There have been reported several experimental studies on the gas-phase reactions of Ti^+ with propane conducted under low and high pressure conditions [11–15]. Using a flow tube reactor technique, Weisshaar and co-workers [11] observed in the high-pressure multiple-collision environment that the primary products at thermal energies were those of H_2 elimination, $TiC_3H_6^+ + H_2$, with the adduct ions $TiC_3H_8^+$ and CH_4 elimination products $TiC_2H_4^+ + CH_4$ found to be relatively small, i.e., 16 and $< 1\%$, respectively. Consistent with the results of Weisshaar [11], the Castleman group [12] also found under high-pressure multiple-collision conditions that the H_2 elimination is the predominant process at thermal energies (91%). Sunderlin and Armentrout [13] studied the $Ti^+ + C_3H_8$ reaction by means of a guided-ion beam mass spectrometer under low-pressure single-collision conditions. These researchers observed that at thermal energies the H_2

Contribution to the Mark S. Gordon 65th Birthday Festschrift Issue.

J. Moc (✉)
Faculty of Chemistry, Wroclaw University,
F. Joliot-Curie 14, 50-383 Wroclaw, Poland
e-mail: jmoc@wchuwr.chem.uni.wroc.pl

M. S. Gordon
Department of Chemistry, Iowa State University,
Ames, IA 50011, USA

elimination products prevailed, with only small amounts of CH_4 elimination detected [13]. The most recent study of the reaction of Ti^+ with propane and deuterated propanes at thermal energies was conducted by the Armentrout group [14]. In the low-pressure single-collision environment of the flow tube, the $TiC_3H_6^+ + H_2$ were again the primary products detected, followed by the $TiC_2H_4^+ + CH_4$, with the product distribution determined to be 98 and 2%, respectively. The dehydrogenation and demethanation of C_3H_8 by Ti^+ were found to be mildly exothermic processes, by 7 ± 3 and 16 ± 3 kcal/mol, respectively [14,15]. Note the more exothermic channel in the case of CH_4 elimination. However, despite the moderate exothermicity of the two elimination channels, the observed reaction efficiency was low, 17% for H_2 loss and $< 1\%$ for CH_4 loss [14].

Following the previous theoretical investigation [10], both density functional theory (DFT) and ab initio calculations have been performed for the $Ti^+ + C_3H_8 \rightarrow TiC_3H_6^+ + H_2$ and $Ti^+ + C_3H_8 \rightarrow TiC_2H_4^+ + CH_4$ elimination reactions. The main goal is to find the most preferred reaction paths for the two cases, and possibly, to indicate the factors contributing to the observed low efficiency of these eliminations, especially CH_4. The present work adds to the systematic studies of structural and reactivity aspects of Ti chemistry [16]. One finding of the preceding study for Ti^++ ethane was that the DFT B3LYP optimized structures of the intermediates and transition states along the reaction paths were generally in acceptable agreement with the corresponding multi-reference ab initio structures [10]. To the current knowledge of the authors, there are only few related computational studies of the reactions between the first row transition metal cation and propane aiming at the elucidation of the detailed mechanisms of both the C–H and C–C activation [17–20]. In fact, all of these calculations involved exclusively late transition metals. Holthausen and Koch [17] studied the reaction of Fe^+ with C_3H_8 at the DFT B3LYP level, whereas Yi et al. [18,19] investigated the $M^+ + C_3H_8$ reactions for M = Ni and Co at the same electronic structure level combined with statistical rate theory. The Co^+ + propane reaction was also examined by Fedorov and Gordon [20] using the multi-reference based CASSCF/MRMP2 ab initio methods and effective core potential on the transition metal.

2 Computational methods

The potential energy surfaces (PESs) of the two elimination reactions were explored with density functional theory (DFT) [21] using the hybrid B3LYP [22–25] functional. Optimized structures were followed by a force constant matrix calculation/diagonalization to confirm the character of the located stationary points [minimum or transition state (TS)] and to provide zero-point energy (ZPE) corrections. The latter corrections are included in the relative energies discussed below (collected in Tables 1, 2). Each transition state was verified to connect a desired pair of minima by tracing the intrinsic reaction coordinate (IRC) [26–32]. These DFT calculations used the valence triple-zeta plus polarization (TZVP) basis set stored internally in GAMESS [33] and described fully in a previous paper [10]. The relative energies have also been calculated with the supplemented Wachters/Pople's basis sets [10,34,35], denoted as WP, and using both the B3LYP and coupled-cluster singles and doubles methods including perturbative triples [CCSD(T)] [36–41]. For WP, the final Ti basis derived from Wachters primitive set [34] and supplemented with diffuse p, d and polarization f functions had the form (15s11p6d2f)/[10s7p4d2f] and it was used in conjunction with Pople's 6-311+G(2d,2p) basis set for C and H [35].

3 Results and discussion

3.1 Reactants and products

The structures of the C_3H_8 reactant and those of the products of dehydrogenation and demethanation of C_3H_8 by Ti^+, $TiC_3H_6^+ + H_2$ and $TiC_2H_4^+ + CH_4$, are shown in Fig. 1. The experimental ground state of Ti^+ is $^4F(4s^13d^2)$ with its lowest doublet state ^2F derived from the same electronic configuration lying 13.2 kcal/mol higher in energy [42]. The DFT B3LYP estimates of the $^2F - ^4F$ splitting of Ti^+ [43] of 14.3 (TZVP) and 13.5 (WP) kcal/mol compare satisfactorily with experiment. As discussed previously [10], the CCSD(T) method with WP basis set predicts the correct ordering of the $^4F(4s^13d^2)$ and $^2F(4s^13d^2)$ states of Ti^+, though it underestimates the $^2F - ^4F$ splitting. The geometric and electronic structure of the CH_4 elimination product $TiC_2H_4^+$ (Fig. 1c) was examined thoroughly in the previous paper as the H_2 elimination product from the Ti^++ ethane reaction [10]. Briefly, B3LYP finds the quartet ($^4B_1$) to be the ground state of $TiC_2H_4^+$ separated from the lowest doublet state ($^2A_1$) by only 2.0 kcal/mol (WP basis). The CCSD(T)/WP energetic order is reversed, i.e., the doublet $^2A_1$ ground-state is 0.2 kcal/mol below the quartet $^4B_1$. In both methods, the two states are nearly degenerate.

The distinct H_2 elimination paths described below resulted in the following elimination product ($TiC_3H_6^+$) isomers: $TiCH_3CHCH_2^+$ (Ti^+-propene), $TiCH_2CH_2CH_2^+$ (Ti^+-cyclopropane) and $TiCHCH_2CH_3^+$ (Fig. 1b). The quartet $TiCH_3CHCH_2^+$ (Ti^+-propene) is found consistently to be the ground-state H_2 elimination product, with the doublet $TiCH_3CHCH_2^+$ lying only 2.5 and 1.2 kcal/mol higher at the B3LYP/WP and CCSD(T)/WP levels of theory. The doublet cyclic isomer $TiCH_2CH_2CH_2^+$ (Ti^+-cyclopropane) is the third most stable H_2 elimination species, placed respectively

Table 1 Relative energies for H_2 elimination paths (kcal/mol)

	B3LYP/TZVP	B3LYP/WP[a]	CCSD(T)/WP[a]
Path1: $Ti^+ + C_3H_8 \rightarrow TiCH_3CHCH_2^+ + H_2$			
Doublet			
$Ti^+ + C_3H_8$	14.3	13.5	
$Ti^+ \cdots C_3H_8$ (**1**)	−8.9	−10.5	−10.3
C–$H^{(2)}$ ins. TS(**TS1-2**)[b]	0.3	−0.6	7.9
$HTiC_3H_7^+$ (**2**)	−16.2	−17.4	−7.7
H_2 elim. TS (**TS2-3**)	−7.8	−9.0	0.6
$TiC_3H_6^+ \cdots H_2$ (**3**)	−11.4	−12.6	−3.1
$TiCH_3CHCH_2^+ + H_2$	−4.7	−5.6	2.1
Quartet			
$Ti^+ + C_3H_8$	0.0	0.0	0.0
$Ti^+ \cdots C_3H_8$ (**1**)	−22.3	−23.5	−17.2
C–$H^{(2)}$ ins. TS(**TS1-2**)[b]	9.8	9.0	18.0
$HTiC_3H_7^+$ (**2**)	7.6	6.8	14.4
H_2 elim. TS (**TS2-3**)	12.2	11.4	21.8
$TiC_3H_6^+ \cdots H_2$ (**3**)	−14.2	−15.3	−4.9
$TiCH_3CHCH_2^+ + H_2$	−7.4	−8.1	0.9
Path2: $Ti^+ + C_3H_8 \rightarrow TiCH_2CH_2CH_2^+ + H_2$			
Doublet			
$Ti^+ + C_3H_8$	14.3	13.5	
$Ti^+ \cdots C_3H_8$ (**4**)	−9.3	−11.1	−5.8
C–$H^{(1)}$ ins. TS(**TS4-5**)[b]	5.1	4.0	11.2
$HTiC_3H_7^+$ (**5**)	−15.3	−16.6	−7.2
H_2 elim. TS (**TS5-6**)	−0.1	−1.6	9.3
$TiC_3H_6^+ \cdots H_2$ (**6**)	−9.9	−10.8	−1.3
$TiCH_2CH_2CH_2^+ + H_2$	−3.9	−4.4	4.8
Quartet			
$Ti^+ + C_3H_8$	0.0	0.0	0.0
$Ti^+ \cdots C_3H_8$ (**4**)	−18.9	−20.3	−13.5
C–$H^{(1)}$ ins. TS(**TS4-5**)[b]	13.6	12.7	19.6
$HTiC_3H_7^+$ (**5**)	13.0	12.1	17.7
H_2 elim. TS (**TS5-6**)	27.7	26.6	36.3
$TiC_3H_6^+ \cdots H_2$ (**6**)	16.1	15.2	25.9
$TiCH_2CH_2CH_2^+ + H_2$	21.6	21.1	32.0
Path3: $Ti^+ + C_3H_8 \rightarrow TiCH_3CHCH_2^+ + H_2$			
Doublet[c]			
$HTiC_3H_7^+$ (**10**)	−13.4	−14.0	−4.3
H migr. TS (**TS10-7**)	−0.5	−1.0	10.4
Dihydrido species (**7**)	−4.3	−4.7	5.7
H_2 elim. TS (**TS7-8**)	4.0	3.6	13.1
$TiC_3H_6^+ \cdots H_2$ (**8**)	−7.0	−7.8	1.6
$TiCH_3CHCH_2^+ + H_2$	−4.7	−5.6	2.1
Quartet[c]			
$Ti^+ \cdots C_3H_8$ (**5a**)	−23.6	−24.6	−17.2
H migr. TS (**TS5a-7**)	41.7	41.0	52.2
Dihydrido species (**7**)	35.1	34.2	47.1
H_2 elim. TS (**TS7-8**)	36.7	35.8	43.8

Table 1 continued

	B3LYP/TZVP	B3LYP/WP[a]	CCSD(T)/WP[a]
$TiC_3H_6^+ \cdots H_2$ (**8**)	−12.6	−13.5	−2.1
$TiCH_3CHCH_2^+ + H_2$	−7.4	−8.1	0.9
Path4: $Ti^+ + C_3H_8 \rightarrow TiCHCH_2CH_3^+ + H_2$			
Doublet			
$Ti^+ + C_3H_8$	14.3	13.5	
$Ti^+ \cdots C_3H_8$ (**9**)	−7.4	−9.0	−6.4
$C–H^{(1)}$ ins. TS(**TS9-10**)[b]	2.9	2.2	10.4
$HTiC_3H_7^+$ (**10**)	−13.4	−14.0	−4.3
H_2 elim. TS (**TS10-11**)	7.4	6.4	14.4
$TiC_3H_6^+ \cdots H_2$ (**11**)	7.2	6.3	14.8
$TiCHCH_2CH_3^+ + H_2$	17.2	16.7	21.1
Quartet			
$Ti^+ + C_3H_8$	0.0	0.0	0.0
$Ti^+ \cdots C_3H_8$ (**9**)	−19.5	−21.1	−15.1
$C–H^{(1)}$ ins. TS(**TS9-10**)[b]	18.5	17.9	25.9
$HTiC_3H_7^+$ (**10**)	15.9	15.3	21.7
H_2 elim. TS (**TS10-11**)	29.0	28.4	37.9
$TiC_3H_6^+ \cdots H_2$ (**11**)	18.6	18.0	28.0
$TiCHCH_2CH_3^+ + H_2$	24.7	24.7	29.2

Energies are relative to the $Ti^+(^4F) + C_3H_8$ ground-state reactants and include ZPE corrections

[a] At the B3LYP/TZVP geometries

[b] $C–H^{(i)}$ means the primary($i = 1$) and secondary ($i = 2$) C–H bond

[c] The first two steps are common with *Path 2*

at 3.7 and 3.9 kcal/mol relative to the ground-state. The quartet cyclic structure $TiCH_2CH_2CH_2^+$ is not competitive energetically, being 29.2 (B3LYP) and 31.1 (CCSD(T)) kcal/mol less stable than the ground state. Another plausible H_2 elimination species, $TiCHCH_2CH_3^+$, obtained from a 1,1 type H_2 elimination reaction from the relevant insertion intermediate (see below) and with Ti^+ bound only to one C atom (Fig. 1b) are high energy structures: at B3LYP/WP (CCSD(T)/WP) they lie 24.8 (20.2) and 32.8 (28.3) kcal/mol above the ground-state for the doublet and quartet, respectively. Although the latter elimination channel is obviously not accessible at thermal energies, the calculated paths will also be presented for comparison.

3.2 Initial complexes

It was mentioned in the Introduction that $Ti^+ \cdots C_3H_8$ adducts/initial complexes were stabilized and detected under multiple-collision conditions [11]. Due to the presence of two terminal CH_3 groups and a central CH_2 group in propane, several $Ti^+ \cdots C_3H_8$ adducts of an ion-induced dipole kind are conceivable. A systematic search led to the η^3 **1**, η^4 **4** and η^3 **9** structures with Ti^+ coordinating to either two or one CH_3 (**4**,**9**) or to both CH_3 and CH_2 (**1**) as shown in Figs. 3, 4, 6 and 7 for the doublet and quartet, respectively. It is important to note that all of these adducts have been confirmed by an IRC to be involved in the respective elimination reaction paths. Additionally, the unique η^3 **5a** quartet adduct (Fig. 6) having all three CH_n groups of propane engaged (one C–H per group) was confirmed by an IRC to be involved in the H_2 elimination path (see below). For the "low-coordinated" η^2 complex **1a** having Ti^+ bound to the central CH_2 (Fig. 2), only the quartet is structurally stable. The doublet structure is a saddle point with a small 30icm^{-1} imaginary mode. As for Ti^+ + ethane [10], the quartet $Ti^+ \cdots C_3H_8$ structures are significantly lower in energy than the doublet analogs (Tables 1, 2). The binding energies (BE) of the lower energy quartet $Ti^+ \cdots C_3H_8$ complexes are within a 4–5 kcal/mol range. The actual BE values are ca. 20–25 kcal/mol (B3LYP/WP) and 14–18 kcal/mol (CCSD(T)/WP) (Tables 1, 2). The binding energy of η^2 **1a**($^4B_1$) complex is 19.9 and 14.5 kcal/mol at B3LYP/WP and CCSD(T)/WP, respectively. Taking into account the expected overbinding by B3LYP [46,47], the two sets of BEs compare reasonably well.

In analogy with the reactions of M^+ with ethane involving the first-row transition metal M^+ cations (M=Ti,Co,Fe)

Table 2 Relative energies for CH_4 elimination paths (kcal/mol)

	B3LYP/TZVP	B3LYP/WP[a]	CCSD(T)/WP[a]
Path1c: $Ti^+ + C_3H_8 \rightarrow TiC_2H_4^+ + CH_4$			
Doublet			
$Ti^+ + C_3H_8$	14.3	13.5	
$Ti^+ \cdots C_3H_8$ (**4**)	−9.3	−11.1	−5.8
C–C ins. TS(**TS4-12**)	14.7	13.6	24.0
$CH_3TiC_2H_5^+$ (**12**)	−28.4	−29.6	−17.1
CH_4 elim. TS (**TS12-13**)	−8.0	−9.3	1.9
$TiC_2H_4^+ \cdots CH_4$ (**13**)	−24.9	−26.2	−17.8
$TiC_2H_4^+ + CH_4$	−14.3	−14.8	−5.2
Quartet			
$Ti^+ + C_3H_8$	0.0	0.0	0.0
$Ti^+ \cdots C_3H_8$ (**4**)	−18.9	−20.3	−13.5
C–C ins. TS(**TS4-12**)	9.3	7.9	20.0
$CH_3TiC_2H_5^+$ (**12**)	1.7	0.8	11.9
CH_4 elim. TS (**TS12-13**)	10.3	8.8	21.8
$TiC_2H_4^+ \cdots CH_4$ (**13**)	−28.3	−29.7	−18.3
$TiC_2H_4^+ + CH_4$	−16.1	−16.8	−4.9
Path2c: $Ti^+ + C_3H_8 \rightarrow TiC_2H_4^+ + CH_4$			
Doublet[b]			
$CH_3TiC_2H_5^+$ (**12**)	−28.4	−29.6	−17.1
H migr. TS (**TS12-14**)	−12.9	−13.8	−0.5
$CH_3TiHC_2H_4^+$ (**14**)	−16.0	−17.0	−4.5
CH_4 elim. TS (**TS14-13**)	−1.2	−2.4	10.2
$TiC_2H_4^+ \cdots CH_4$ (**13**)	−24.9	−26.2	−17.8
$TiC_2H_4^+ + CH_4$	−14.3	−14.8	−5.2
Quartet[b]			
$CH_3TiC_2H_5^+$ (**12a**)	3.3	2.3	11.7
CH_4 elim. (**TS12a-13**)	23.4	22.5	32.5
$TiC_2H_4^+ \cdots CH_4$ (**13**)	−28.3	−29.7	−18.3
$TiC_2H_4^+ + CH_4$	−16.1	−16.8	−4.9
Path3c: $Ti^+ + C_3H_8 \rightarrow TiC_2H_4^+ + CH_4$			
Doublet[c,d]			
$HTiC_3H_7^+$ (**5**)	−15.3	−16.6	−7.2
CH_3 migr. TS (**TS5-14**)	−5.8	−7.2	4.1
Quartet[c]			
$HTiC_3H_7^+$ (**5**)	13.0	12.1	17.7
CH_3 migr. TS(**TS5-14**)	36.9	35.7	43.7
$CH_3TiHC_2H_4^+$ (**14**)	16.5	15.5	24.8
CH_4 elim. TS (**TS14-13**)	18.3	17.1	27.8
$TiC_2H_4^+ \cdots CH_4$ (**13**)	−28.3	−29.7	−18.3
$TiC_2H_4^+ + CH_4$	−16.1	−16.8	−4.9

Energies are relative to the $Ti^+(^4F) + C_3H_8$ ground-state reactants and include ZPE corrections

[a] At the B3LYP/TZVP geometries

[b] The first two steps are common with *Path1c* (plus isom. of **12** to **12a** for the quartet path)

[c] The first two steps are common with *Path2*

[d] The last two steps are common with *Path2c*

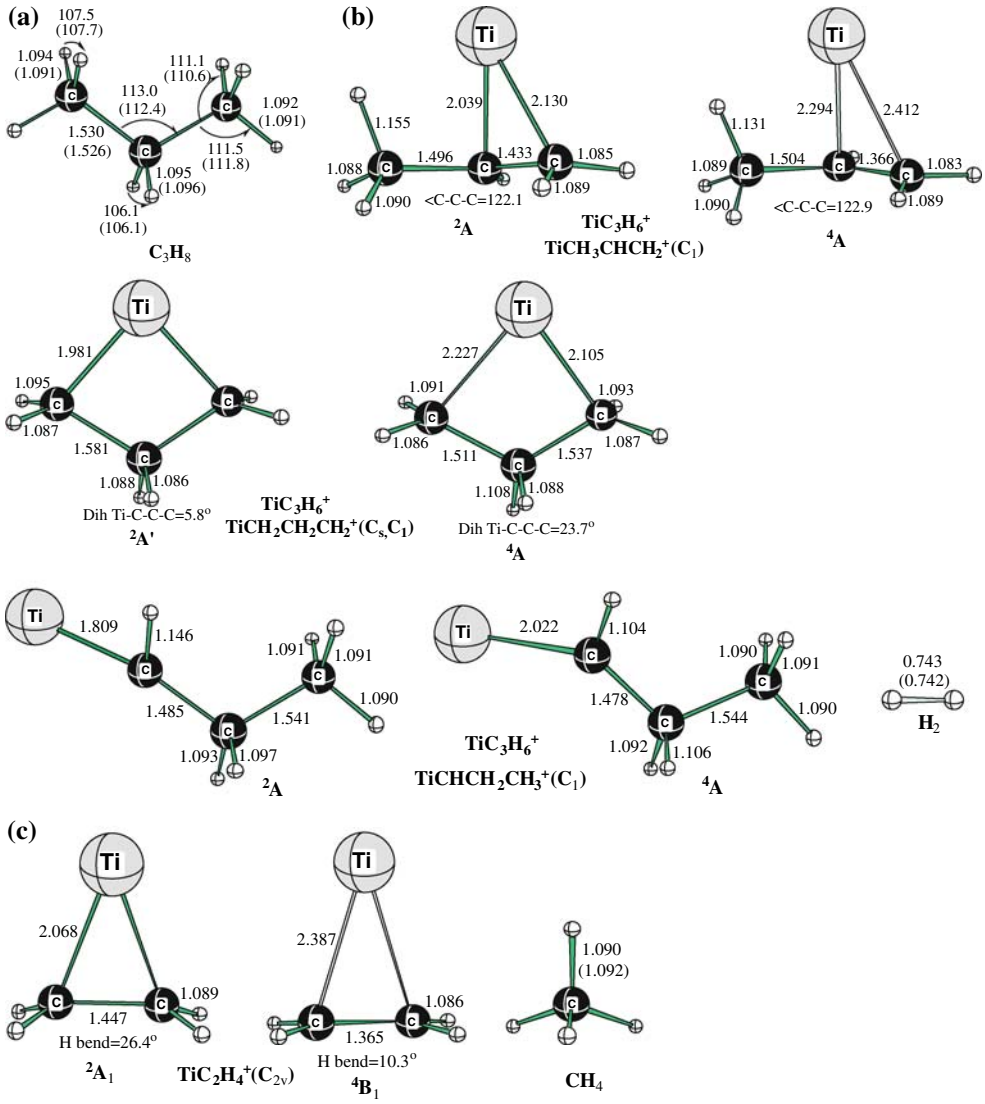

Fig. 1 Structures of **a** C_3H_8 reactant, **b** various H_2 elimination products, and **c** CH_4 elimination products from the $Ti^+ + C_3H_8$ reaction (bond lengths in Å). For $TiC_2H_4^+$, H bend denotes the out-of-plane bending angle of the H atoms (0^o for the isolated C_2H_4). Values in *parentheses* are from experiment (taken from references [44,45])

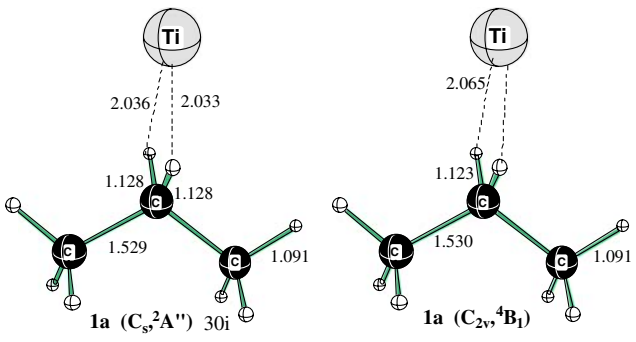

Fig. 2 The initial $Ti^+ \cdots C_3H_8$ complex structures not involved in the elimination paths (bond lengths in Å); magnitude of imaginary frequency (cm^{-1}) for the doublet complex is shown

[10,46,47], for Ti^+ + propane, the relevant $Ti^+ \cdots C_3H_8$ complex initiates a subsequent Ti^+ insertion, into a primary (C–$H^{(1)}$) or secondary (C–$H^{(2)}$) C–H bond or C–C bond of propane. Based on the results for Ti^++ ethane [10], the quartet and doublet PESs for C–H activation in propane are expected to cross early in the reaction coordinate (r.c.). This expectation arises from the significantly higher energy of the quartet C–H insertion intermediates relative to the doublet analogs. Furthermore, since some doublet and quartet H_2/CH_4 elimination products from the $Ti^+ + C_3H_8$ reaction have similar relative energies, the spin crossing between the quartet and doublet PESs can also occur in the vicinity of the exit channel. In this work, the doublet and quartet PESs have been calculated systematically along the respective paths.

The structures involved in the H_2/CH_4 elimination reactions are shown in Figs. 3, 4 and 5 (doublet) and Figs. 6, 7 and 8 (quartet). The same labels are used for the corresponding doublet and quartet structures (except for some unique cases). Because there is a substantial degree of similarity between the B3LYP/TZVP geometric parameters of the species involved in the Ti^++ ethane [10] and Ti^++ propane reactions, the discussion below primarily focuses on the mechanistic and energetic issues for the latter process.

3.3 H_2 elimination

The energy profiles for H_2 elimination paths examined are denoted *Pathi* ($i = 1 - 4$) and drawn in Figs. 9a–d. These profiles are calculated based on the B3LYP energies and each *Pathi* includes the high- and low-spin PESs, essential to predict the lowest energy path. The corresponding CCSD(T) energy profiles have been shown in Figs. 10a–d. The CCSD(T)/WP versus B3LYP/WP relative energies for the various intermediates and transition states involved are compared in Table 1.

3.3.1 Path1

Path1 involves the reaction sequence **1** → **TS1-2** → **2** → **TS2-3** → **3** → $TiCH_3CHCH_2^+ + H_2$ (Figs. 3, 6, 9a). The energy profile of *Path1* bears close resemblance to that for dehydrogenation of ethane by Ti^+ [10]. There is, especially, double spin crossing along the r.c.: first, between the initial complex and secondary C–H insertion transition state, and second, after passing the H_2 elimination TS. Both crossings take place below the $Ti^+(^4F) + C_3H_8$ asymptote, at least according to B3LYP (Fig. 9a). At low energies, the first spin crossing could turn the reaction to the lower energy doublet PES, on which the energetically most favorable C–H insertion TS is located. This is on condition that the strongly enough spin-orbit coupling occurs [10]. As explained earlier [10], switching to the low-spin PES enables forming a stable insertion species by singlet coupling a pair of electrons to form Ti–C(Ti–H) bonds. Conserving the high spin does not permit forming strong covalent bonds [10] and the quartet reaction intermediates show significantly longer Ti–C distances compared to the doublet analogs (up to 0.4 Å).

Thus, for *Path1*, the insertion occurs into the $C–H^{(2)}$ bond and leads to the doublet intermediate $HTiC_3H_7^+$ **2** via the **TS1-2** transition state (oxidative addition). As the next step on the doublet PES, the molecular complex $TiCH_3CHCH_2^+ \cdots H_2$ **3** is formed via the four-center 1,2 H_2 elimination transition state **TS2-3**. Because, on the quartet surface, the complex **3** formation step is significantly exothermic (by 22.1 kcal/mol at B3LYP/WP with respect to **2**) and results in the more stable quartet structure compared to the doublet analogue, the second spin crossing occurs in this region. The final step is the endothermic H_2 release from **3** (Fig. 9a). The overall H_2 elimination reaction $Ti^+(^4F) + C_3H_8 \rightarrow TiCH_3CHCH_2^+(^4A) + H_2$ is calculated at B3LYP/WP to be mildly exothermic, by 8.1 kcal/mol, in reasonable agreement with experiment (7 ± 3 kcal/mol) [14]. At this computational level, the rate-limiting doublet transition state **TS1-2** is located slightly below (0.6 kcal/mol) the $Ti^+(^4F) + C_3H_8$ asymptote. CCSD(T)/WP (Fig. 10a) finds the overall reaction to be essentially thermoneutral ($\Delta E_o = 0.9$ kcal/mol), while the barrier for the doublet $C–H^{(2)}$ bond insertion is located at this level 7.9 kcal/mol above the ground-state reactant energy. It is well known that DFT underestimates barrier heights, so these results are consistent with that observation. However, the doublet-quartet crossings are predicted by the two methods to occur in the same regions.

3.3.2 Path2

Path2 involves the reaction sequence **4** → **TS4-5** → **5** → **TS5-6** → **6** → $TiCH_2CH_2CH_2^+ + H_2$ (Figs. 3, 6, 9b), with an early spin crossing analogous to *Path1* (Fig. 9b). CCSD(T), Fig. 10b, exhibits similar spin crossing. The doublet insertion takes place into the primary C–H bond via the **TS4-5** transition state, resulting in the intermediate **5** (Fig. 9b). The subsequent formation of H_2 proceeds through the four-center 1,3 H_2 elimination**TS5-6** and leads to the dihydrogen complex $TiCH_2CH_2CH_2^+ \cdots H_2$ **6**. The latter contains the cyclic product $TiCH_2CH_2CH_2^+$, left after releasing H_2. The quartet PES remains significantly shifted upward after the spin crossover, ending endothermically (Fig. 9b). The energetically most favorable channel within *Path2*, $Ti^+(^4F) + C_3H_8 \rightarrow TiCH_2CH_2CH_2^+(^2A') + H_2$, is formally spin-forbidden, with a B3LYP/WP exothermicity of 4.4 kcal/mol, ca. half that of *Path1*. At CCSD(T)/WP (Fig. 10b), this reaction is slightly endothermic, by 4.8 kcal/mol (Table 1). Compared to *Path1*, *Path2* appears also less favorable kinetically because the rate-limiting doublet transition state **TS4-5** involved in the latter is located 4.0 (11.2) kcal/mol above the $Ti^+(^4F) + C_3H_8$ asymptote, based on the B3LYP/WP [CCSD(T)/WP] calculations.

3.3.3 Path3

The first two steps of *Path3* including the spin crossing and yielding the $C–H^{(1)}$ insertion intermediate $HTiC_3H_7^+$ **5** (Fig. 9c) are common with *Path2*. On the doublet surface, **5** can rearrange to the somewhat less stable isomer **10** (Fig. 3), differing primarily by the Ti-C-C-C dihedral angle (the latter isomer is also involved in *Path4*, see below). Attempts to locate the corresponding isomerization TS failed. The IRC calculation confirmed that starting with **10**, further rearrangement via the H migration transition state **TS10-7** leads to the dihydrido intermediate $H_2TiC_3H_6^+$ **7** (Fig. 3). Interestingly,

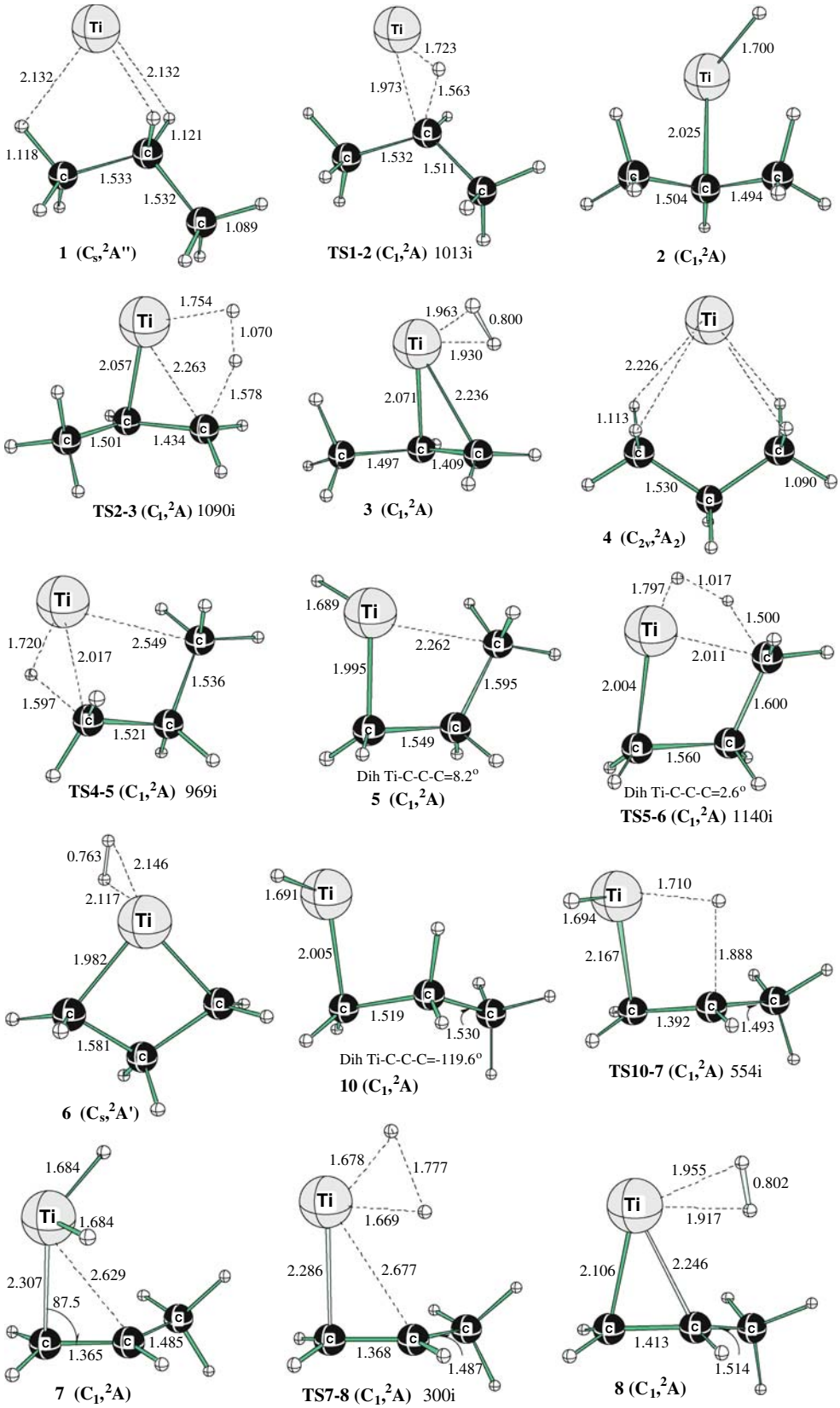

Fig. 3 Doublet structures relevant to the H_2 elimination of C_3H_8 by Ti^+ and starting with the η^3 **1** and η^4 **4** $Ti^+ \cdots C_3H_8$ initial complexes, respectively (bond lengths in Å, bond angles in degrees); for TS's, the associated imaginary frequencies (cm^{-1}) are given

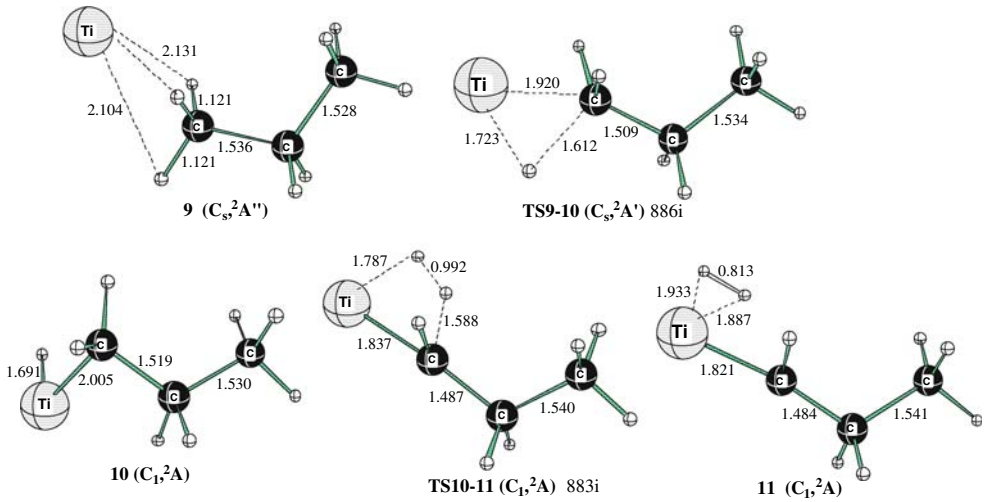

Fig. 4 Doublet structures relevant to the H_2 elimination of C_3H_8 by Ti^+ and starting with the η^3 **9** $Ti^+ \cdots C_3H_8$ initial complex (bond lengths in Å); for TS's, the associated imaginary frequencies (cm^{-1}) are given

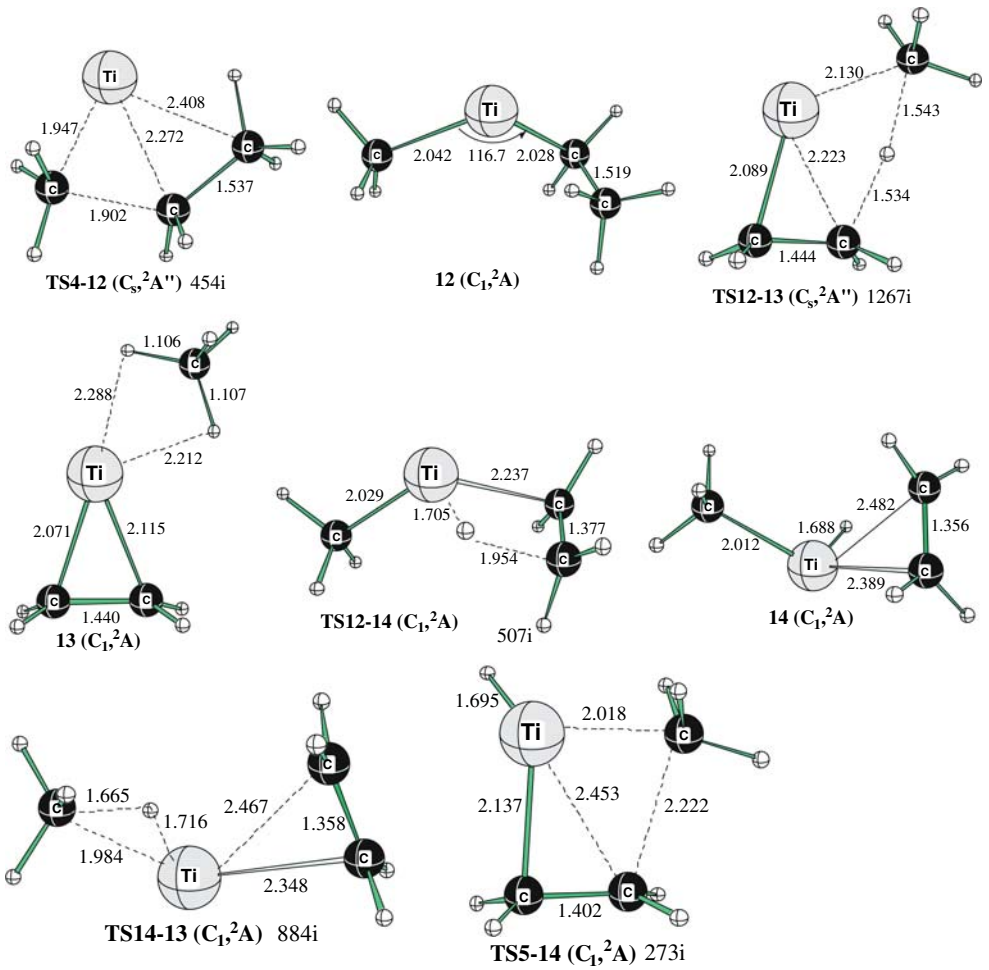

Fig. 5 Doublet structures relevant to the CH_4 elimination of C_3H_8 by Ti^+ (bond lengths in Å, bond angles in degrees); for TS's, the associated imaginary frequencies (cm^{-1}) are given

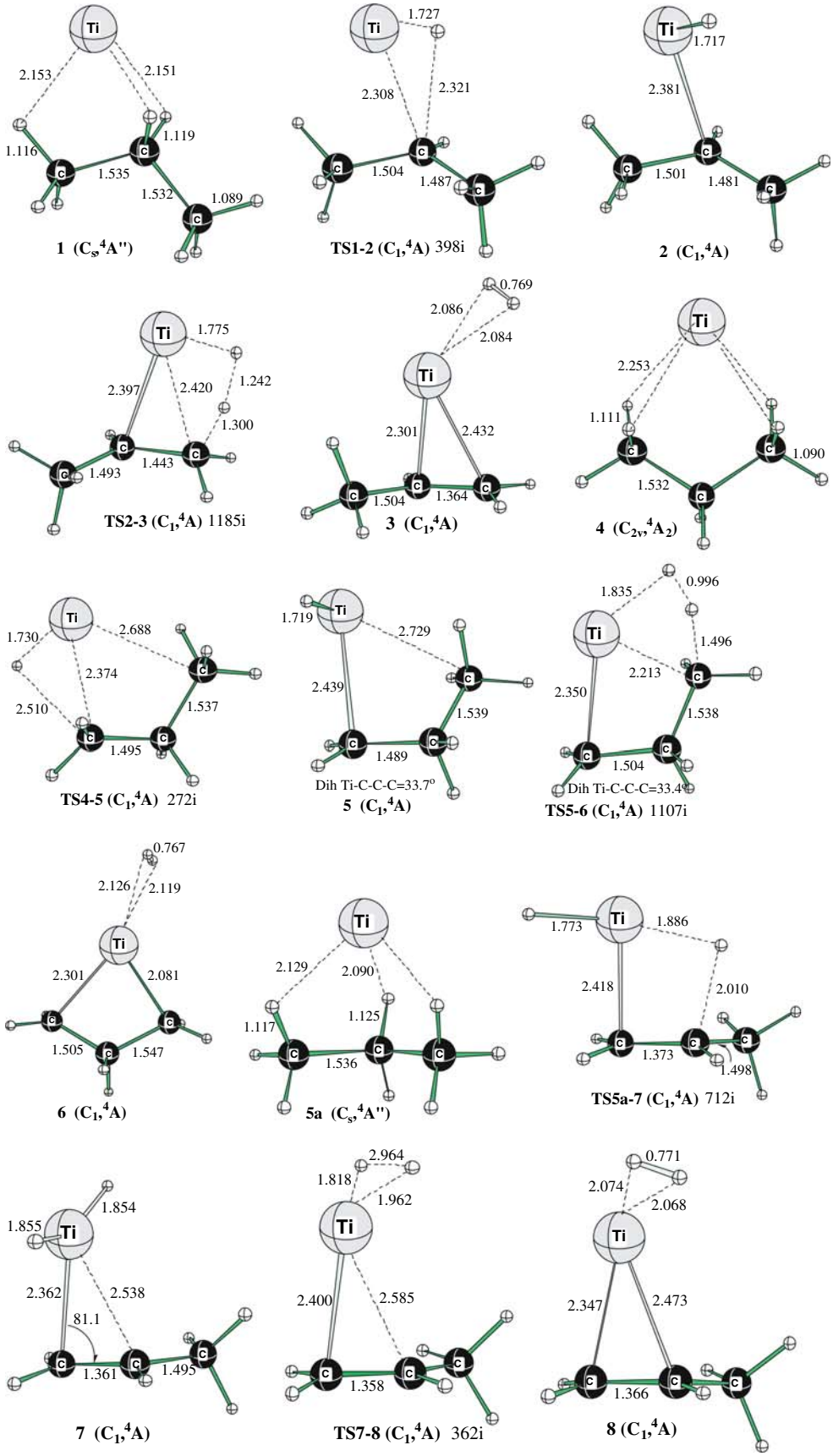

Fig. 6 Quartet structures relevant to the H_2 elimination path analogs of the doublet paths described in Fig. 3 (bond lengths in Å, bond angles in degrees); for TS's, the associated imaginary frequencies (cm^{-1}) are given

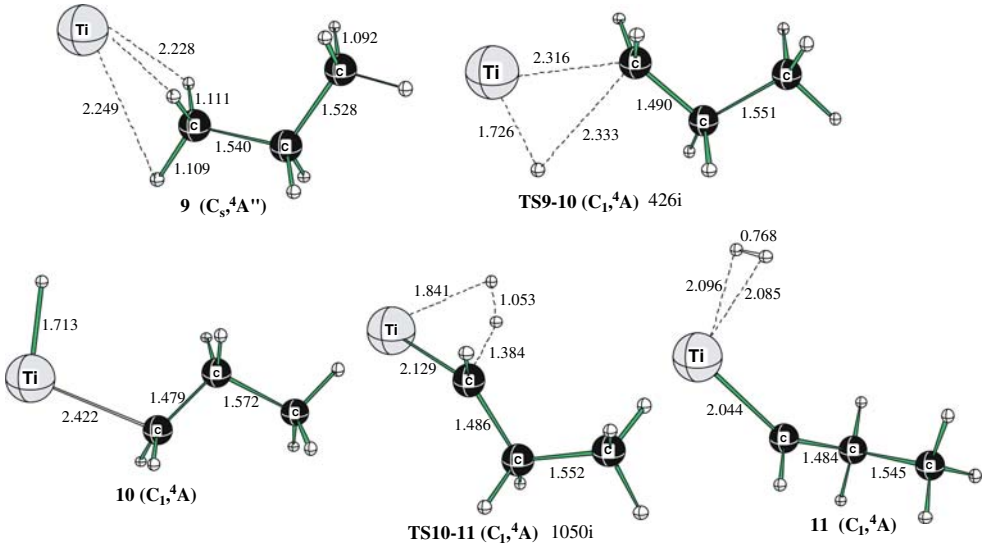

Fig. 7 Quartet structures relevant to the H_2 elimination path analogs of the doublet paths described in Fig. 4 (bond lengths in Å, bond angles in degrees); for TS's, the associated imaginary frequencies (cm^{-1}) are given

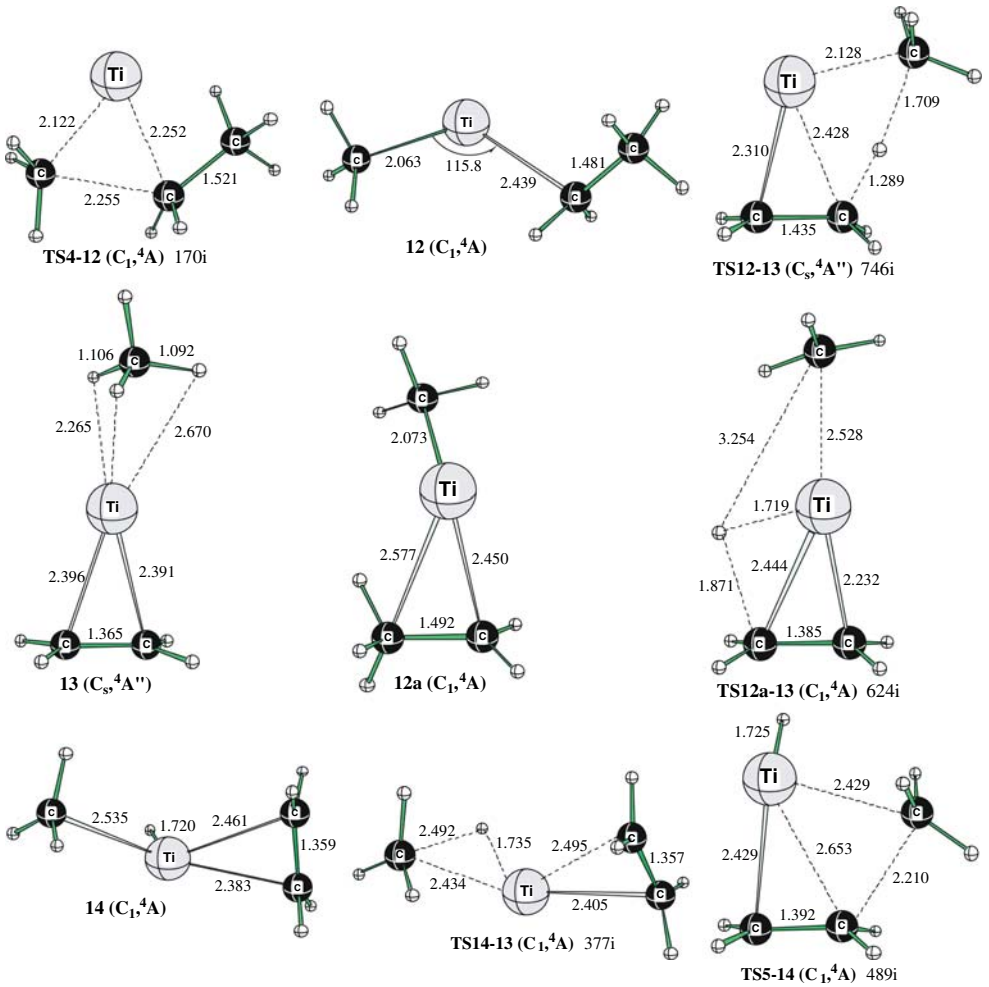

Fig. 8 Quartet structures relevant to the CH_4 elimination path analogs of the doublet paths described in Fig. 5 (bond lengths in Å, bond angles in degrees); for TS's, the associated imaginary frequencies (cm^{-1}) are given

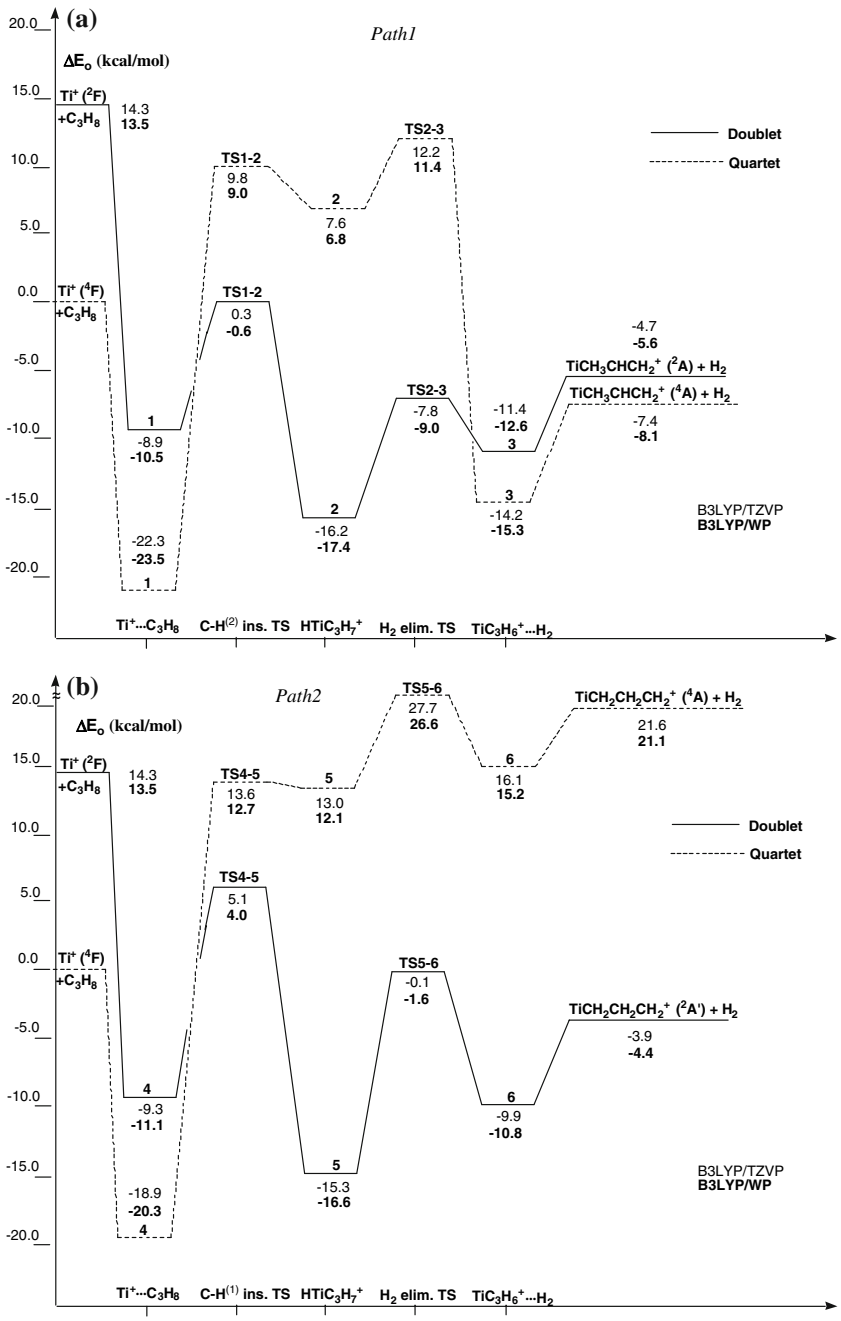

Fig. 9 The B3LYP energy profiles for the $Ti^+ + C_3H_8 \rightarrow TiC_3H_6^+ + H_2$ reaction corresponding to **a** *Path1*, **b** *Path2*, **c** *Path3* and **d** *Path4*

this kind of intermediate was postulated by experimentalists [8,14]. However, for the $M^+ + C_3H_8$ reactions involving M = Fe and Ni, the existence of the dihydrido structure as a minimum on the PES was not supported [17,18]. At the B3LYP/WP level of theory, the dihydrido species **7**and **TS10-7** directly leading to it both lie below the ground-state reactant energy, by 4.7 and 1.0 kcal/mol, respectively. CCSD(T)/WP (Fig. 10c) locates the two structures somewhat above this asymptote, by 5.7 and 10.4 kcal/mol (Table 1). Towards the exit channel, **7** can transform via **TS7-8** to the dihydrogen complex $TiCH_3CHCH_2^+ \cdots H_2$ **8**, from which H_2 is expelled. Note that **8** shows the H_2 fragment in the *cis* position with respect to the CH_3 group, unlike its more stable isomer **3**, involved in *Path1*, having H_2 unit in the *trans* position.

On the quartet PES, dihydrido species **7** is highly unstable (Fig. 9c). The IRC calculation revealed that the immediate transition state involved, **TS5a-7**, connects to the $Ti^+ \cdots C_3H_8$ complex **5a** instead of to the quartet analog of **10**. Consequently, the predicted reaction step from **5a** to **7** requires overcoming a large energetic barrier. Similar to

Fig. 9 continued

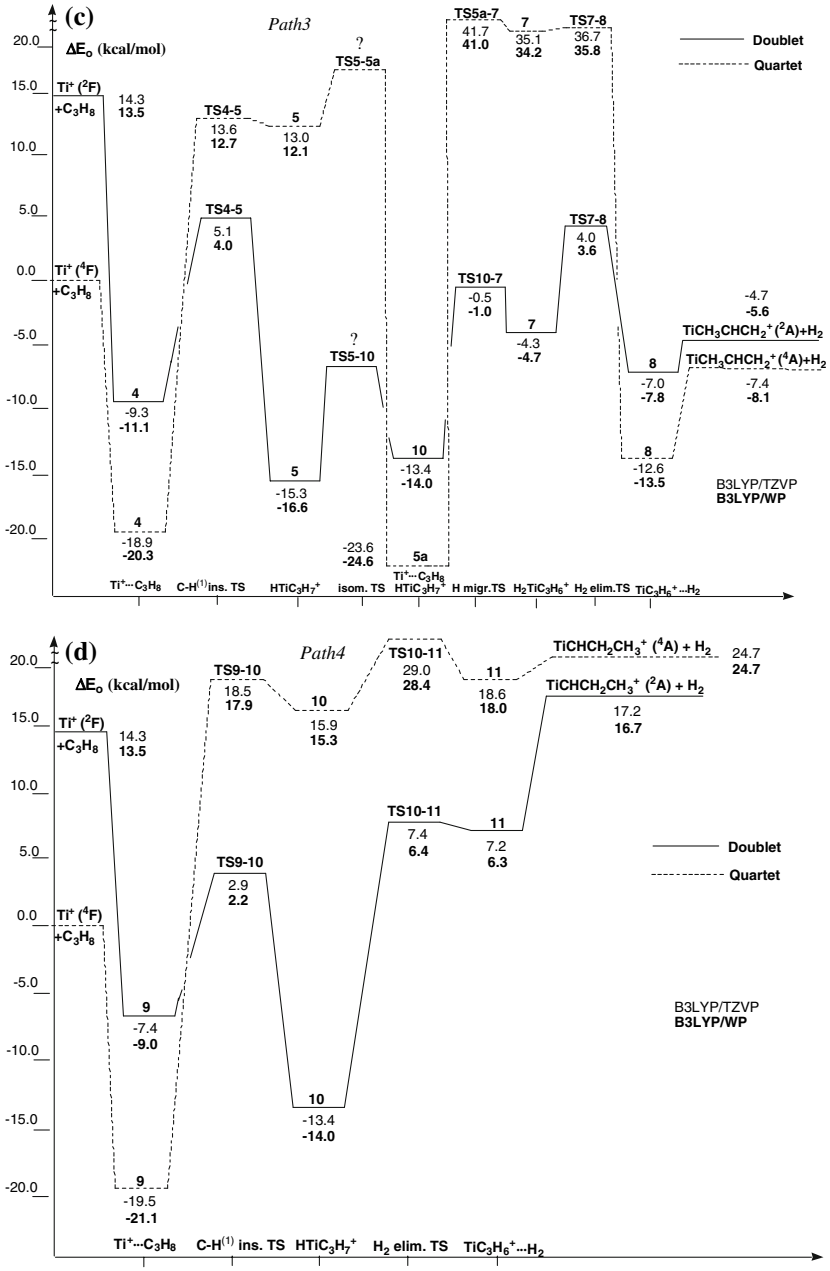

Path1, the following step leading to the elimination products precursor $TiCH_3CHCH_2^+ \cdots H_2$ **8** is appreciably exothermic on the quartet PES (by 47.7 kcal/mol relative to **7**at B3LYP/WP), which crosses the doublet surface after passage of **TS7-8**. The exit channel of *Path3* corresponds to that of *Path1*. *Path3* is consistent with the general stepwise mechanism for $M^+ + C_3H_8$ reaction originally suggested by experimentalists [8,14]. At B3LYP/WP, the rate-limiting TS of *Path3* is the same as for *Path2*, whereas with CCSD(T)/WP, the H_2 elimination **TS7-8** is the highest energy point on the doublet PES lying 13.1 kcal/mol above $Ti^+(^4F) + C_3H_8$ (Table 1, Fig. 10c).

3.3.4 Path4

Path4 (Figs. 4, 7, 9d) is similar to *Path2* in that there is a single spin crossing early at r.c. - between the initial η^3 adduct **9** and C–$H^{(1)}$ insertion transition state **TS9-10**—and that the quartet surface is mostly shifted above the doublet one. The insertion step produces directly the intermediate **10**, involved also in *Path3* (note a different view of doublet structure **10** in Figs. 3, 4). The B3LYP/WP(CCSD(T)/WP) barrier height at the doublet **TS9-10** amounts to 2.2 (10.4) kcal/mol relative to the quartet reactants, which is only 2.9 (2.5) kcal/mol larger than the net energy requirement at the doublet **TS1-2**

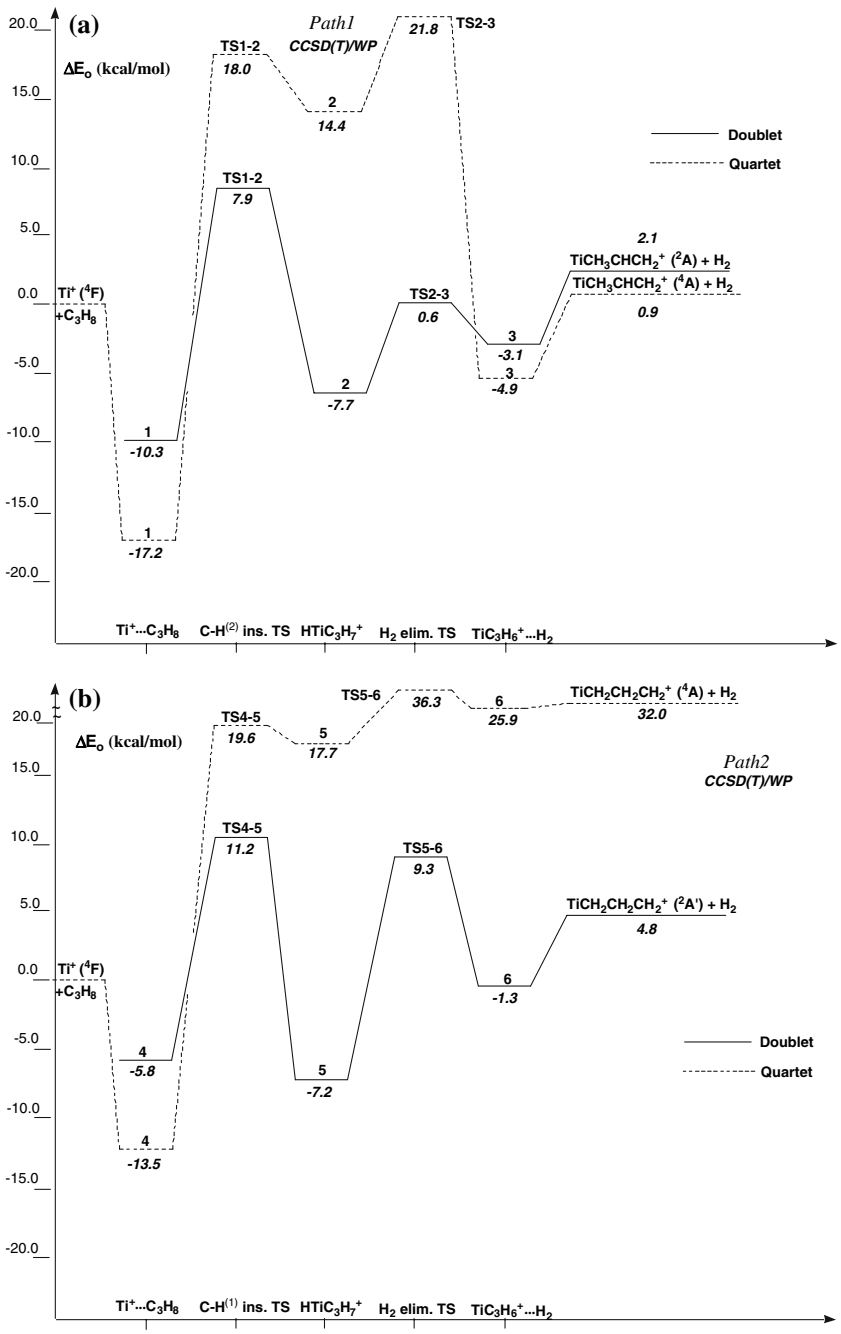

Fig. 10 The CCSD(T) energy profiles for the $Ti^+ + C_3H_8 \rightarrow TiC_3H_6^+ + H_2$ reaction corresponding to **a** *Path1*, **b** *Path2*, **c** *Path3* and **d** *Path4*

belonging to *Path1* (Table 1). Nevertheless, the remainder of *Path4* proceeding on the lower energy doublet PES is less favorable, ending especially with the endothermic products obtained from **10** by 1,1 H_2 elimination through **TS10-11** (Fig. 9d, Table 1).

It appears from the above comparison, that the three routes *Pathi* ($i = 1 - 3$) involve an "early" quartet-doublet spin crossing (we neglect the endothermic *Path4*), with *Path1* and *Path3* found to have the largest exothermicity. The rate-limiting TS located on the doublet PES reachable by the prior efficient spin crossing is found to be either for C–H insertion or H_2 elimination, depending on the path and the method. For *Path1*, the associated net barrier which corresponds to the secondary C–H insertion is predicted to be the lowest and ranges from −0.6 (B3LYP/WP) to 7.9 (CCSD(T)/WP) kcal/mol. One can thus conclude that the H_2 elimination *Path1* is expected to be most favoured at low energies. The two methods agree qualitatively, although the CCSD(T) PES is shifted upward by several kcal/mol.

Fig. 10 continued

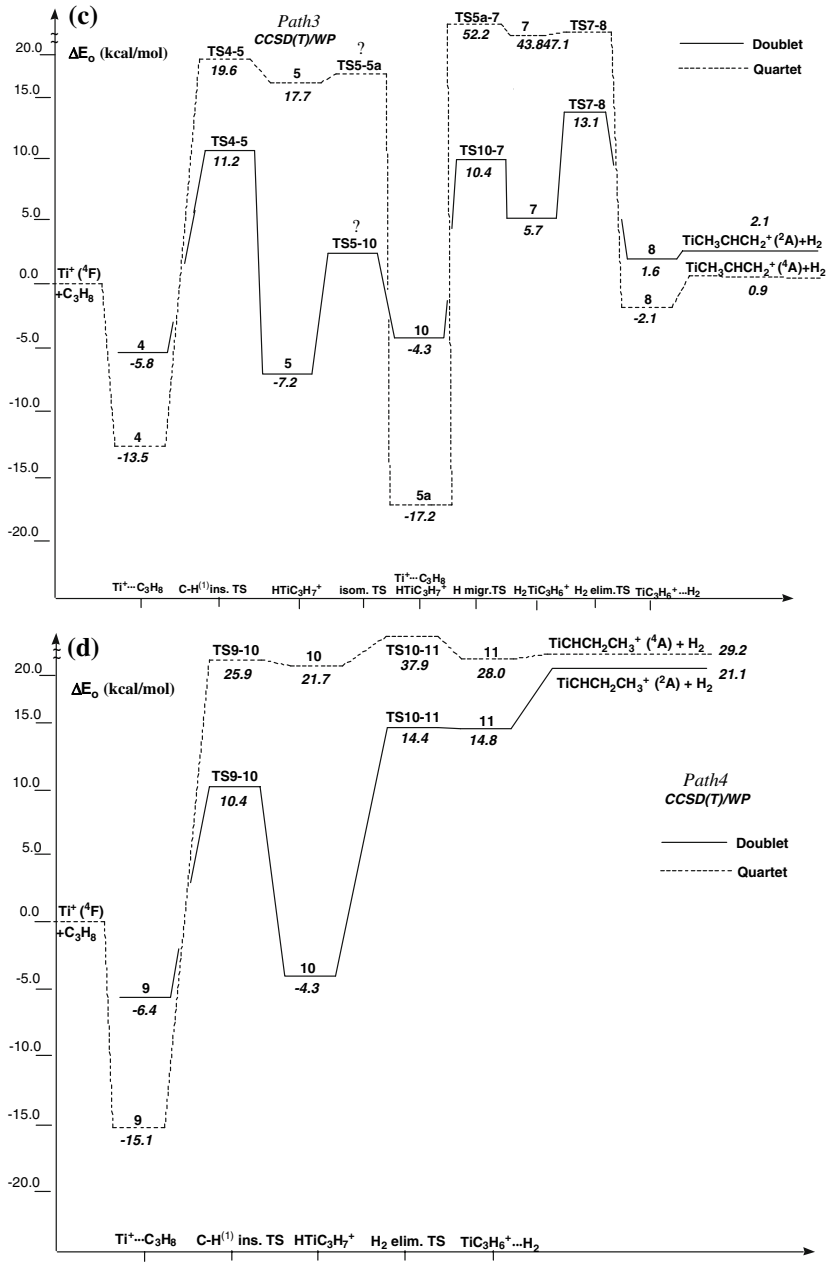

3.4 CH_4 elimination

The CH_4 elimination energy profiles are named *Pathic* ($i = 1-3$) and presented in Figs. 11a–c (B3LYP) and Figs. 12a–c (CCSD(T)). Both *Path1c* and *Path2c* involve an initial C–C insertion, whereas *Path3c* involves the initial primary C–H bond insertion shared with *Path2* for H_2 loss. The three paths begin with the η^4 **4** adduct formation.

3.4.1 Path1c

Path1c involves the reaction sequence **4** → **TS4-12** → **12** → **TS12-13** → **13** → $TiC_2H_4^+ + CH_4$ (Figs. 3, 4, 5, 6, 8, 11a, 12a). After passing the C–C insertion transition state **TS4-12**, the quartet PES crosses for the first time the doublet PES and this apparently occurs above the $Ti^+(^4F) + C_3H_8$ asymptote (Figs. 11a, 12a). The lower energy doublet PES in this region leads to the very stable $CH_3TiC_2H_5^+$ **12** insertion intermediate (the global minimum), lying ca. 30 kcal/mol [17 for CCSD(T)] below the $Ti^+(^4F) + C_3H_8$ reactants. The energy profile featuring the C–C insertion product "deep well" resembles that of demethanation of C_2H_6 by Ti^+ [10]. In the next step on the doublet surface, $CH_3TiC_2H_5^+$ **12** is transformed to the molecular complex $TiC_2H_4^+ \cdots CH_4$ **13** via the CH_4 elimination transition state **TS12-13** (Figs. 5, 11a). The latter step on the quartet surface appears to be

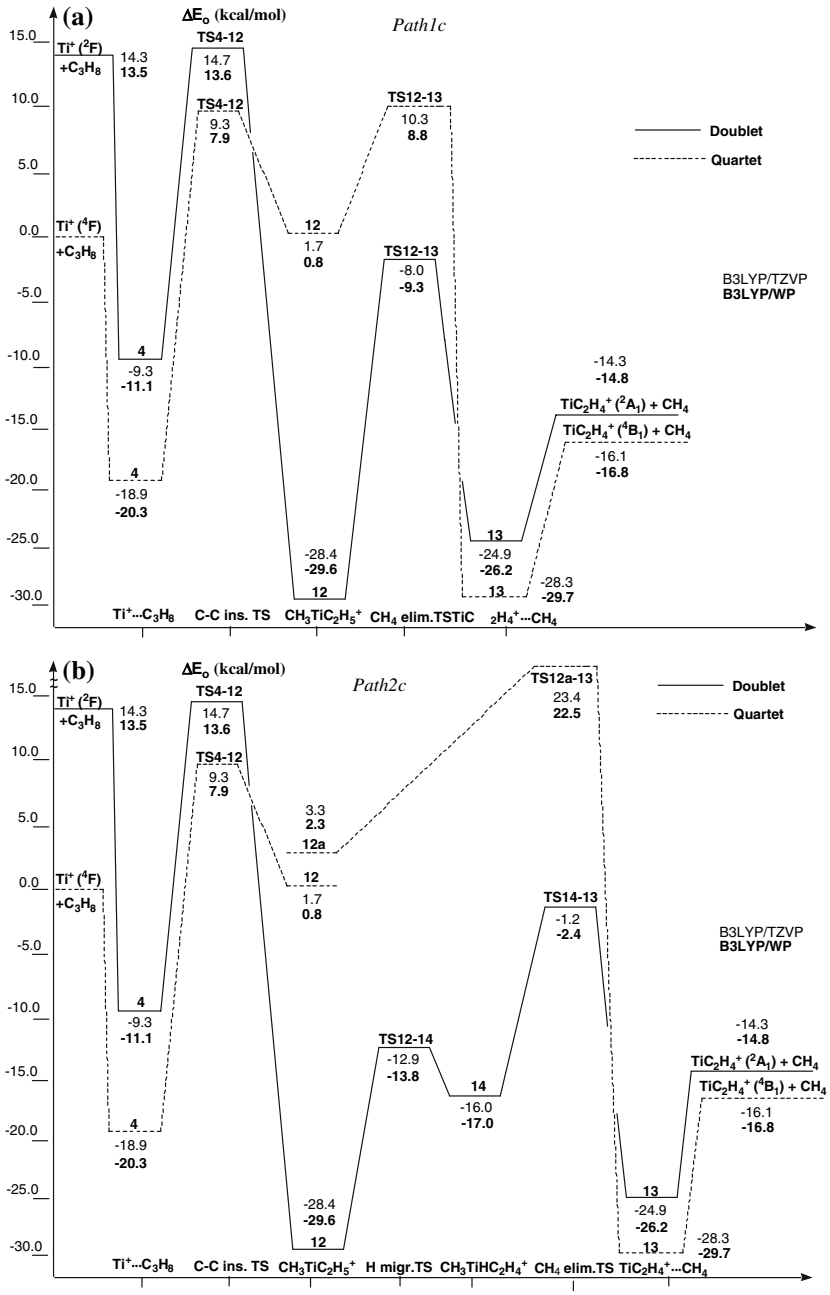

Fig. 11 The B3LYP energy profiles for the $Ti^+ + C_3H_8 \rightarrow TiC_2H_4^+ + CH_4$ reaction corresponding to **a** *Path1c*, **b** *Path2c* and **c** *Path3c*

significantly exothermic (by 30.5 kcal/mol at B3LYP/WP and 30.2 kcal/mol for CCSD(T) relative to **12**) which results in the more stable quartet structure **13** relative to the doublet counterpart and second spin crossing (Fig. 11a). The endothermic CH_4 release from **13** ends *Path1c*. Note that according to CCSD(T)/WP (Fig. 12a) this is accompanied by another spin crossing because the doublet products lie at this level 0.2 kcal/mol below the quartet ones (Table 2).

The overall CH_4 elimination reaction $Ti^+(^4F) + C_3H_8 \rightarrow TiC_2H_4^+(^4B_1) + CH_4$ is found at B3LYP/WP to be exothermic by 16.8 kcal/mol, in reasonable agreement with experiment (16 ± 3 kcal/mol) [14,15]. At this level of theory, the rate-limiting C–C insertion quartet transition state **TS4-12** is placed 7.9 kcal/mol above the $Ti^+(^4F) + C_3H_8$ asymptote. The CCSD(T)/WP predicted exothermicity is 5.2 kcal/mol [with the $TiC_2H_4^+(^2A_1) + CH_4$ products], whereas the barrier for the quartet C–C bond insertion is located 20 kcal/mol above the ground-state reactant energy (Table 2).

3.4.2 *Path2c*

The first two steps of *Path2c* (Figs. 11b, 12b) are the same as for *Path1c*. Along *Path2c*, the common insertion intermediate $CH_3TiC_2H_5^+$ **12** rearranges on the doublet PES to

Fig. 11 continued

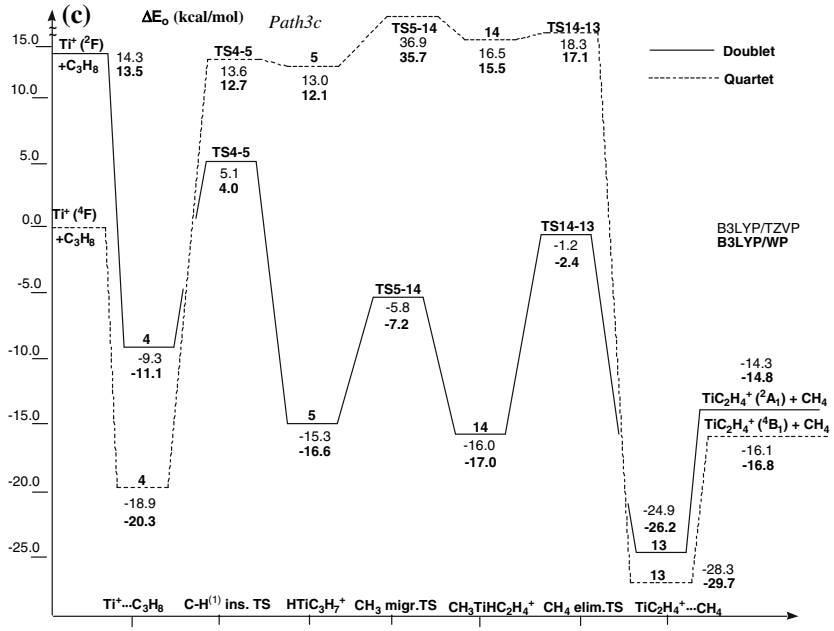

the $CH_3TiHC_2H_4^+$ species **14** via an H migration transition state **TS12-14** (Fig. 5). At B3LYP/WP, **14** and **TS12-14** are below the $Ti^+(^4F) + C_3H_8$ reference, by 17.0 and 13.8 kcal/mol, respectively. CCSD(T)/WP locates the two structures also below this reference, by 4.5 and 0.5 kcal/mol (Table 2; Fig. 12b). The doublet intermediate **14** can eliminate CH_4 through the transition state **TS14-13** to yield the molecular complex $TiC_2H_4^+ \cdots CH_4$ **13**.

On the quartet PES, starting from $CH_3TiC_2H_5^+$, the mechanism of CH_4 elimination is different. In this case a single step is needed to transform the $CH_3TiC_2H_5^+$ intermediate to the CH_4 precursor. It begins rather with its isomer **12a** and leads directly to the complex $TiC_2H_4^+ \cdots CH_4$ **13** via **TS12a-13** as confirmed by the IRC (Figs. 8, 11b). Despite careful searching, we were not able to locate the **12** → **12a** isomerization TS. As anticipated from the *Path1c* profile, the rearrangement from **12a** to **13** is accompanied by the second spin crossing (Fig. 11b). Obviously, the exit channel here looks like that for *Path1c*.

3.4.3 Path3c

For *Path3c*, the C–$H^{(1)}$ bond insertion step is shared with *Path2* (*Path3*) for H_2 loss. Starting from the doublet insertion intermediate **5**, the key step of *Path3c* is the CH_3 group migration via **TS5-14** to form the $CH_3TiHC_2H_4^+$ intermediate **14**, the latter already encountered along *Path2c* (Fig. 5, Fig. 11c). Therefore, the remainder of *Path3c* on the doublet PES, starting from **14**, corresponds to *Path2c*. Between **5** and **14**, the quartet PES lies some 12–36 kcal/mol (B3LYP/WP) above the $Ti^+(^4F) + C_3H_8$ asymptote. Transforming the quartet **14** to $TiC_2H_4^+ \cdots CH_4$ via **TS14-13** leads to a second spin crossing in the region of the exit channel (Fig. 11c).

Although, the overall CH_4 elimination reaction exothermicity of *Path3c* is the same as for *Path1c* and *Path2c*, the three paths differ kinetically. For the last two routes, the rate-limiting TS is that for C–C insertion, located on the quartet PES and lying 7.9 (B3LYP/WP) and 20 kcal/mol [CCSD(T)/WP] above $Ti^+(^4F) + C_3H_8$. For *Path3c*, the rate-limiting TS is located on the doublet PES. According to B3LYP/WP it is for the primary C–H insertion with the net barrier of 4.0 kcal/mol. With CCSD(T)/WP, the doublet TS heights for primary C–H insertion (11.2 kcal/mol) and CH_4 elimination (10.2 kcal/mol) of *Path3c* are within 1 kcal/mol and are thus both candidates for the rate-limiting TS (Table 2). The three paths feature a second "late" spin crossing in the vicinity of the exit channel; though only for *Path1c* and *Path3c* this is expected to occur below the $Ti^+(^4F) + C_3H_8$ asymptote. At low energies, the CH_4 elimination *Path3c* is thus most likely.

4 Conclusions

The following major conclusions can be inferred from the detailed exploration of PES for the reactions of H_2 and CH_4 elimination of C_3H_8 by Ti^+:

(i) The lowest energy path for H_2 elimination (*Path1*) involves an initial Ti^+ insertion into a secondary C–H bond on the doublet PES. This step must be preceded by the quartet-doublet spin crossing. An additional "late" spin crossing occurs in the region of the exit channel. At B3LYP/WP, the overall $Ti^+(^4F) + C_3H_8 \rightarrow TiCH_3CHCH_2^+(^4A) + H_2$ reaction is found to be exothermic by 8.1 kcal/mol. The rate-limiting TS, for the secondary C–H insertion, is located at

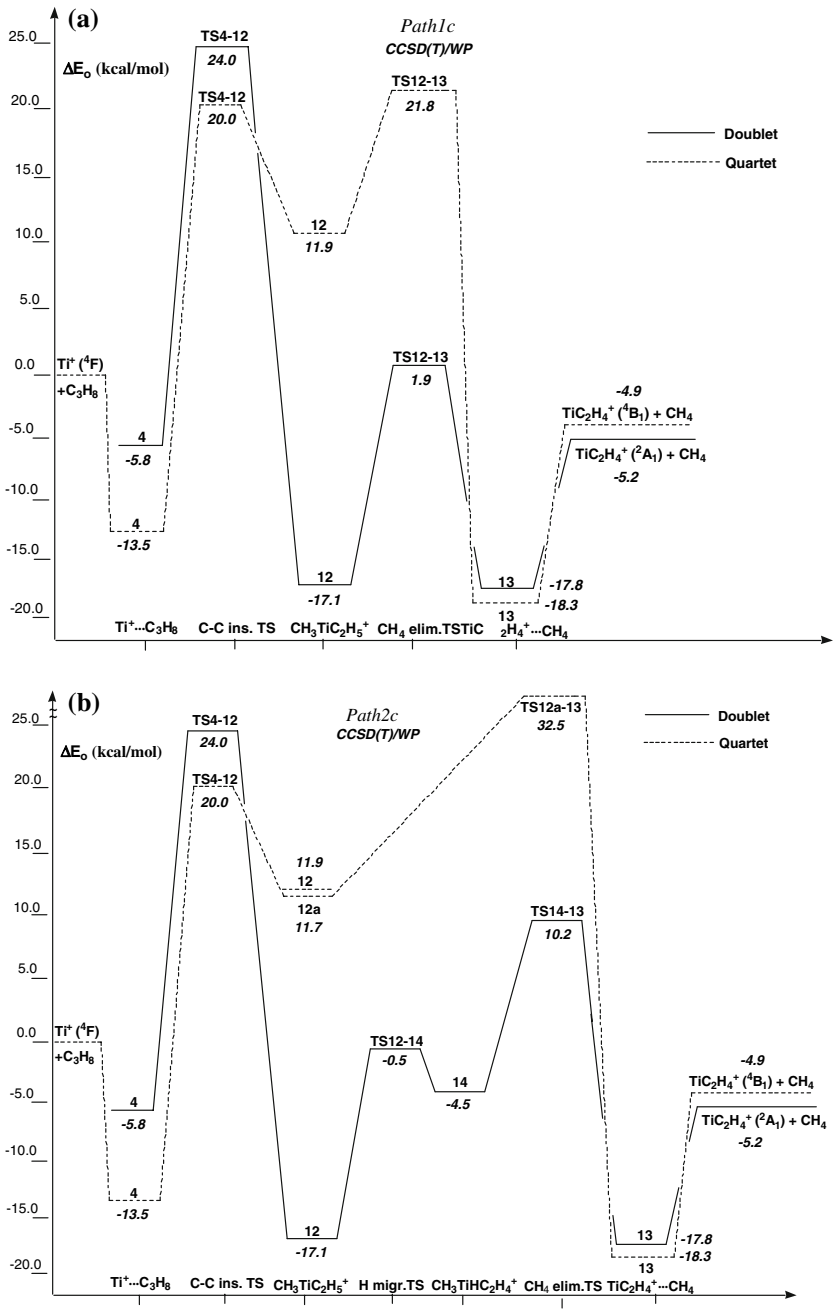

Fig. 12 The CCSD(T) energy profiles for the $Ti^+ + C_3H_8 \rightarrow TiC_2H_4^+ + CH_4$ reaction corresponding to **a** *Path1c*, **b** *Path2c* and **c** *Path3c*

this level 0.6 kcal/mol below the $Ti^+(^4F) + C_3H_8$ reference. CCSD(T)/WP finds the overall elimination reaction to be essentially thermoneutral with the corresponding barrier of the same rate-limiting TS of 7.9 kcal/mol.

(ii) The lowest energy path for CH_4 elimination (*Path3c*) involves an initial Ti^+ insertion into primary C–H bond on the doublet PES. This step must be preceded by a spin crossing. Second [and third at CCSD(T)/WP] "late" spin crossings also take place along the path. With B3LYP/WP [CCSD(T)/WP], the overall $Ti^+(^4F) + C_3H_8 \rightarrow TiC_2H_4^+(^4B_1) + CH_4$ ($TiC_2H_4^+(^2A_1) + CH_4$) reaction exothermicity is calculated as 16.8 (5.2) kcal/mol. The B3LYP/WP rate-limiting TS, for the primary C–H insertion, is located 4.0 kcal/mol above the $Ti^+(^4F) + C_3H_8$ reference. According to CCSD(T)/WP, the doublet TSs along *Path3c* for primary C–H insertion and CH_4 elimination with the respective heights of 11.2 and 10.2 kcal/mol are both candidates for the rate-limiting TS.

(iii) The observed [14] at thermal energies low efficiency of the two eliminations, especially CH_4, can be caused by multiple spin crossings required along the lowest energy paths. To discuss this effect quantitatively, both the precise location of the spin crossings, especially those lying above the $Ti^+(^4F) + C_3H_8$ asymptote, and Ti spin-orbit coupling matrix element estimate are needed [10].

Fig. 12 continued

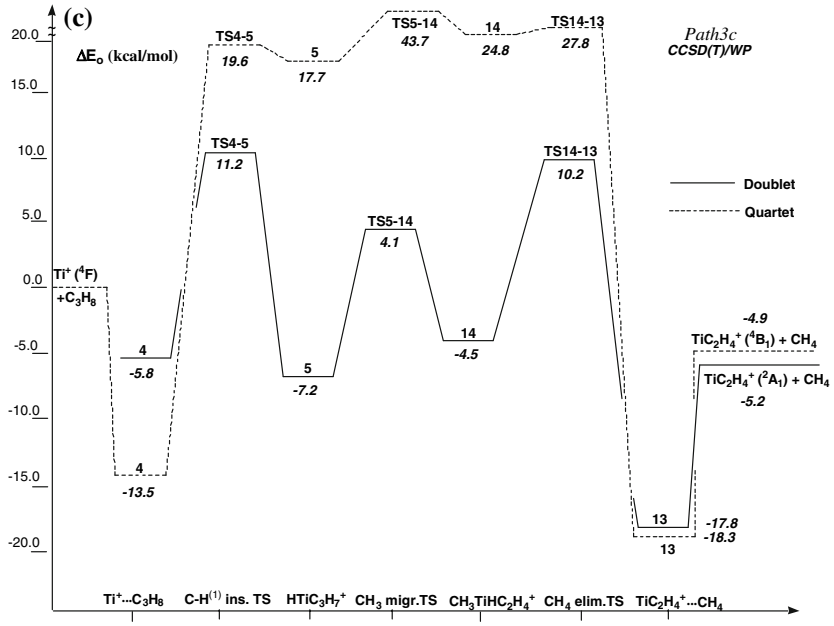

References

1. Eller K, Schwarz H (1991) Chem Rev 91:1121
2. Schröder D, Schwarz H (1995) Angew Chem Int Ed Engl 34:1973
3. Böhme DK, Schwarz H (2005) Angew Chem Int Ed Engl 44:2336
4. van Koppen PAM, Kemper PR, Bowers MT (1996) In organometallic ion chemistry. In: Freiser BS (ed) Kluwer, Dordrecht, p 157
5. Armentrout PB (1989) In gas-phase inorganic chemistry. In: Russell DH (ed) Plenum Press, New York, p 1
6. Armentrout PB (1990) In selective hydrocarbon activation: principles and progress. In: Davies JA, Watson PL, Liebman J, Greenberg A (eds) VCH, New York, p 467
7. Weisshaar JC (1992) In advances in chemical physics. In: Ng C (ed) Wiley Interscience, New York, vol 82, pp 213–261
8. Van Koppen PAM, Bowers MT, Fisher ER, Armentrout PB (1994) J Am Chem Soc 116:3780 and papers cited therein
9. Siegbahn PEM (1996) In advances in chemical physics. In: Prigogine I, Rice SA (eds) Wiley, New York, vol XCIII, pp 333–386
10. Moc J, Fedorov DG, Gordon MS (2000) J Chem Phys 112:10247
11. Tonkyn R, Ronan M, Weisshaar JC (1988) J Phys Chem 92:92
12. MacTaylor RS, Vann WD, Castleman AW Jr (1996) J Phys Chem 100:5329
13. Sunderlin LS, Armentrout PB (1989) Int J Mass Spect Ion Process 94:149
14. Van Koppen PAM, Bowers MT, Haynes CL, Armentrout PB (1998) J Am Chem Soc 120:5704
15. Sievers MR, Jarvis LM, Armentrout PB (1998) J Am Chem Soc 120:1891
16. Gordon MS, Bode BM, Webb SP, Kudo T, Moc J, Fedorov DG, Chung G (2001) Titanium chemistry in computational organometallic chemistry. In: Cundari TR (ed) Marcel Dekker Inc, New York, pp 275–290
17. Holthausen MC, Koch W (1996) Helv Chimica Acta 79:1939
18. Yi SS, Blomberg MRA, Siegbahn PEM, Weisshaar JC (1998) J Phys Chem A 102:395
19. Yi SS, Reichert EL, Holthausen MC, Koch W, Weisshaar JC (2000) Chem Eur J 6:2232
20. Fedorov DG, Gordon MS (2000) J Phys Chem A 104:2253
21. Becke AD (1988) Phys Rev A 38:3098
22. Becke AD (1993) J Chem Phys 98:1372
23. Becke AD (1993) J Chem Phys 98:5648
24. Lee C, Yang W, Parr RG (1988) Phys Rev B 37:785
25. Vosko SH, Wilk L, Nusair M (1980) Can J Phys 58:1200
26. Fukui K (1981) Acc Chem Res 14:363
27. Ishida K, Morokuma K, Komornicki A (1977) J Chem Phys 66:2153
28. Schmidt MW, Gordon MS, Dupuis M (1985) J Am Chem Soc 107:2585
29. Garrett BC, Redmon MJ, Steckler R, Truhlar DG, Baldridge KK, Bartol D, Schmidt MW, Gordon MS (1988) J Chem Phys 92:1476
30. Baldridge KK, Gordon MS, Steckler R, Truhlar DG (1989) J Chem Phys 93:5107
31. Gonzalez C, Schlegel HB (1989) J Chem Phys 90:2154
32. Gonzalez C, Schlegel HB (1990) J Phys Chem 94:5523
33. GAMESS (General Atomic and Molecular Electronic Structure System): Schmidt MW, Baldridge KK, Boatz JA, Elbert ST, Gordon MS, Jensen JH, Koseki S, Matsunaga N, Nguyen KA, Su S, Windus TL, Dupuis M, Montgomery JA Jr (1993) J Comput Chem 14:1347
34. Wachters AJH (1970) J Chem Phys 52:1033
35. Frisch MJ, Pople JA, Binkley JS (1984) J Chem Phys 80:3265
36. Cizek J (1969) Adv Chem Phys 14:35
37. Purvis GD, Bartlett RJ (1982) J Chem Phys 76:1910
38. Scuseria GE, Janssen CL, Schaefer HF III (1988) J Chem Phys 89:7382
39. Raghavachari K, Trucks GW, Pople JA, Head-Gordon M (1989) Chem Phys Lett 157:479
40. Scuseria GE, Schaefer HF III (1989) J Chem Phys 90:3700
41. Watts JD, Gauss J, Bartlett RJ (1993) J Chem Phys 98:8718
42. Sugar J, Corioliss, C (1985) J Phys Chem Ref Data 14 (Suppl. No. 2)
43. Hay PJ (1977) J Chem Phys 66:4377
44. Lide DR (1960) J Chem Phys 33:1514
45. Hehre WJ, Radom L, Schleyer PvR, Pople JA (1986) Ab initio molecular orbital theory. Wiley, New York
46. Holthausen MC, Fiedler A, Schwarz H, Koch W (1996) J Phys Chem 100:6236
47. Holthausen MC, Koch W (1996) J Am Chem Soc 118:9932